D10488

ADVMEW
ISSN 0935-9648
Vol. 20, No. 21
November 3, 2008

ADVANCED MATERIALS

WILEY-VCH

Strain-Engineered Micro-/Nanotubes on Polymers

DOI: 10.1002/adma.200801589

Versatile Approach for Integrative and Functionalized Tubes by Strain Engineering of Nanomembranes on Polymers**

By *Yongfeng Mei,* Gaoshan Huang, Alexander A. Solovev, Esteban Bermúdez Ureña, Ingolf Mönch, Fei Ding, Thomas Reindl, Ricky K. Y. Fu, Paul K. Chu,* and *Oliver G. Schmidt*

Flexible electronics,[1] extremely sensitive sensors,[2] strained-silicon technology,[3] and macromolecule separation,[4] are only a few examples stimulating increasing interest in free-standing nanomembranes, which can be fabricated out of thin solid films,[1–5] particle nanocomposites,[2,6] organic layers,[7] organic/inorganic networks,[8] and even graphene sheets.[9] Strain engineering offers an advanced strategy to deterministically rearrange such nanomembranes into three-dimensional micro-/nanostructures[10] including tubes,[11–18] helices,[11,19,20] rings,[21,22] wrinkles[10,23] and other advanced microarchitectures,[24,25] all of which serve for applications in electronics,[25,26] mechanics,[22] fluidics,[23,27] and photonics.[16,28] The fabrication often requires a selective underetching procedure to release the nanomembranes from their substrate, which heavily constraints the number of desirable materials for exciting applications in, e.g., metamaterials[29,30] or biomedical[31] research. The material choice is limited, because the selective underetching not only removes the underlying sacrificial layer but also in many cases dissolves the nanomembrane material itself.

We circumvent this problem for a broad range of materials and material combinations by a new approach outlined in Figure 1a. A pre-stressed inorganic nanomembrane deposited at low temperatures onto a polymer sacrificial layer (here: photoresist) is released from the substrate surface by removing the sacrificial layer with a solvent (here: acetone), and rolls-up into a micro- or nanotube. Acetone etches (dissolves) a polymer layer over almost any inorganic material with practically 100% selectivity, and examples of rolled-up tubes are shown in Figure 1b–i for various materials and material combinations: b) Pt, c) Pd/Fe/Pd, d) TiO_2, e) ZnO, f) Al_2O_3, g) Si_xN_y, h) Si_xN_y/Ag, and i) diamond-like carbon (DLC). Tubes of well-defined length and geometry can be arranged into large periodic arrays as demonstrated for SiO/SiO_2 microtubes on a Si substrate in Figure 1j. The tube diameter can be tuned by changing the thickness and the built-in strain of the nanomembranes[32] as shown in Figure 1k. If we simplify the layer system to a bilayer of the same material[17] with equal layer thicknesses ($t/2$) and an abrupt strain difference ($\Delta\varepsilon$) at the interface between the two layers, the diameter (D) can be described by the dashed lines in Figure 1k for various $\Delta\varepsilon$. While our simplification provides a rough estimate of the strain state inside the film, it is obvious that unlike to epitaxial defect free films an accurate analytical description of the measured diameter is not possible. We identify three major parameters influencing the strain state and thus the diameter of the rolled-up nanomembranes: (i) difference in the thermal expansion between sacrificial layers and deposited films controlled by substrate temperature, (ii) deposition rate, and (iii) stress evolution during deposition, itself. By choosing appropriate parameters we can exert accurate control over the tube diameter for a certain film thickness as shown in Figure 1k for Al_2O_3, Ti, and Si_xN_y tubes. The parameters are not fully decoupled from each other, and advanced strain engineering is required for every new material and material combination in non-epitaxial films.[33]

First we exploit the difference in thermal expansion controlled by choosing appropriate deposition temperatures. It is well known that thermal stresses are caused by the difference in thermal expansion coefficients (TEC) of deposited films and substrates.[33] For instance, if we deposit thick inorganic nanomembranes (>100 nm) with low TEC on thick polymer layers with 1–2 orders of magnitude larger TECs, the nanomembranes form into wrinkled structures upon detachment from the substrate (not shown). This behavior is clear evidence of built-in compressive strain in the attached nanomembrane with no or only a small stress gradient present in the layer.[23] In order to enhance the stress gradient by the thermal expansion effect, we increase the substrate temperature for the initial part of the layer deposition. For the Al_2O_3

[*] Dr. Y. F. Mei, Dr. G. S. Huang, A. A. Solovev, E. Bermúdez Ureña, Dr. I. Mönch, F. Ding, Prof. O. G. Schmidt
Institute for Integrative Nanosciences, IFW Dresden
Helmholtzstr. 20, 01069 Dresden (Germany)
E-mail: y.mei@ifw-dresden.de
T. Reindl
Max-Planck-Institut für Festkörperforschung
Heisenbergstrasse 1, 70569 Stuttgart (Germany)
Dr. R. K. Y. Fu, Prof. P. K. Chu
Department of Physics and Materials Science, City University of Hong Kong, Tat Chee Avenue, Hong Kong SAR (P. R. China)

[**] We are grateful for experimental help by Dominic J. Thurmer, Francesca Cavallo, Ronny Engelhard, Emica Coric, Barbara Eichler, Cornelia Krien, Sandra Sieber, and Dr. Jill S. Becker; and helpful discussions with Peter Cendula, Dr. Yuanfu Chen, Dr. Juliane Gabel, Dr. Christoph Deneke, Dr. Mohamed Benyoucef, Dr. Suwit Kiravittaya, and Dr. Armando Rastelli. Fruitful discussions with Christine Schmidt, Cancer Research UK are acknowledged. This work was financially supported by the BMBF (No. 03X5518) and Hong Kong Research Grants Council (RGC) General Research Funds (GRF) (No. CityU112307). Supporting Information is available online from Wiley InterScience or from the authors.

 © 2008 WILEY-VCH Verlag GmbH & Co. KGaA, Weinheim

ADVANCED MATERIALS

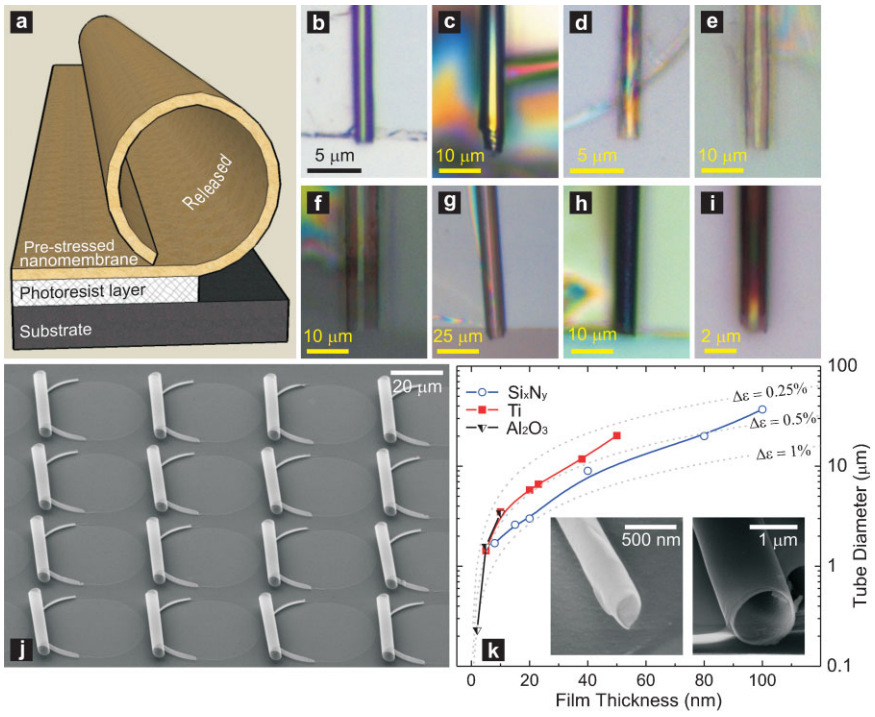

Figure 1. a) Schematic diagram illustrating the roll-up process of a nanomembrane into a tube on photoresist; optical images of rolled-up nanomembranes made out of b) Pt, c) Pd/Fe/Pd, d) TiO_2, e) ZnO, f) Al_2O_3, g) Si_xN_y, h) Si_xN_y/Ag, and i) DLC; j) SEM image of an array of rolled-up SiO/SiO_2 nanomembranes; k) tube diameters as a function of film thickness for various materials: Si_xN_y (blue open circles), Ti (red filled squares), and Al_2O_3 (black half-filled triangles). Left inset shows an SEM image of an Al_2O_3 tube with a diameter of ~230 nm. Right inset displays an SEM image of a Si_xN_y microtube.

layers shown in Figure 1k, the substrate temperature was kept at 80 °C for the bottom part and room temperature for the top part of the layers consisting of two equally thick layers. This technique exerts good and predictable control over the strain state during film deposition and the built-in strain is roughly estimated to be $\Delta\varepsilon = 0.5\%$ in our simple bilayer model. The minimum diameter obtained by this technique is ~230 nm and the opening of the tube is shown as a left inset in Figure 1k.

The second important deposition parameter, especially for evaporation or sputtering, is the deposition rate. For the Ti bilayers, the bottom layer with a thickness of $t/2$ was deposited at 4 Å s^{-1} and the top layer at 0.2 Å s^{-1} with the same thickness of $t/2$ at room temperature. Different deposition rates may lead to different grain sizes in the layers,[33] which in turn exert different stress levels in the nanomembrane. The tube diameter as a function of the film thickness agrees with the curve for a strain difference of 0.5%, which implies that the stress state is well-controllable by tuning the growth rate.

Finally, the relaxation and build-up of strain during deposition, itself,[29] can lead to sufficiently large strain gradients to cause the roll-up process. Figure 1k displays the diameter of Si_xN_y microtubes as a function of film thickness. The films are deposited at 85 °C at constant rate on the polymer layer by plasma-enhanced chemical vapor deposition (PE-CVD). As the film thickness increases, complicated mechanisms to both release and build up stress in certain parts of the film occur.[33] This interplay between relaxation and generation of stress[17] creates a strain gradient in the Si_xN_y nanomembrane responsible for the roll-up process. The strain in nonepitaxial films is too complicated to clearly identify and separate one mechanism from the other, but it should be possible to further optimize deposition conditions to enhance the strain gradient within the nanomembranes to achieve even smaller diameters.

For accurate positioning and tube integration on a single chip, we apply two simple processes for two fundamentally different deposition techniques. As outlined in Figure 2a and b, tilted deposition is used for normal physical vapor deposition methods such as e-beam or thermal evaporation as well as sputtering deposition. In this case a narrow gap remains open after deposition at the far end of the patterned polymer layer due to the ballistic shadow effect that always occurs in glancing angle deposition (GLAD).[34] The solvent can enter through this gap and removes the sacrificial polymer layer from one side. As a result the strained nanomembrane rolls up into a well-defined direction as demonstrated for Ti/Au microtubes in Figure 2c. The length and number of rotations are given by the initial size and geometry of the covered polymer pattern.

Because of the excellent conformity of layers deposited by CVD and atomic layer deposition (ALD), the simple shadow effect cannot be used. Instead, we apply standard lithography and processing technology as sketched in Figure 2d. After depositing nanomembranes by PE-CVD or ALD (Fig. 2d(i)), a second lithography/etching step is carried out to open a window at one side of the covered polymer layer (ii–iii). In our experiments we used 25% H_3PO_4 solution to selectively remove parts of the Al_2O_3 layers. The solvent can enter through this window and removes the polymer layer in such a way that the nanomembrane rolls-up into one well-defined direction (iii). Figure 2e shows an optical microscope image of a directionally rolled-up Al_2O_3 microtube processed by the above steps.

In the following we have selected examples from four different scientific fields to give a flavor of the broad range of possible applications accessible by our technology. Figure 3 shows a typical photoluminescence spectrum from a rolled-up SiO/SiO_2 microtube with a diameter of ~5.5 μm excited by a 532 nm laser line at room temperature. Pronounced optical modes occur[28] and are denoted in the spectrum with their azimuthal mode number. The mode intensities and positions

© 2008 WILEY-VCH Verlag GmbH & Co. KGaA, Weinheim

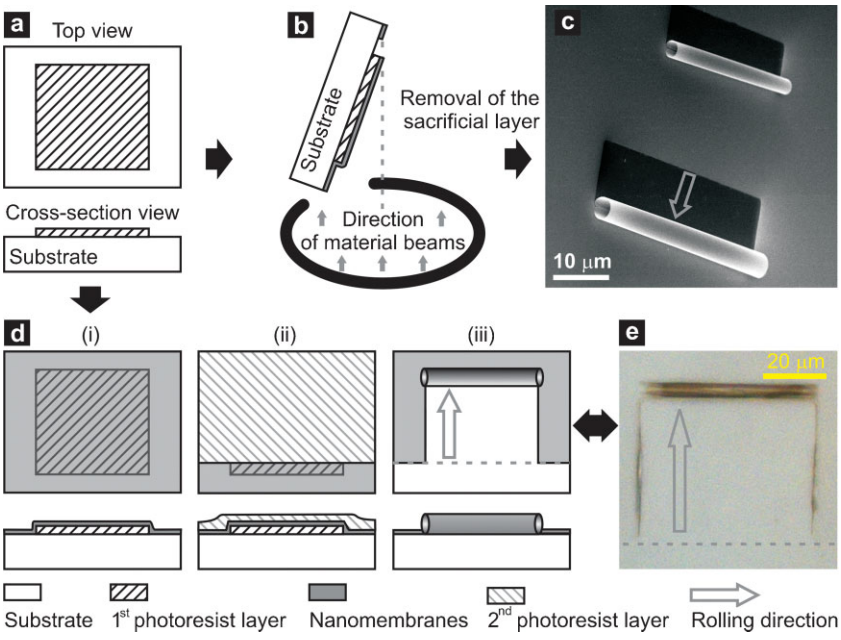

Figure 2. Process flow for positioning rolled-up nanomembranes. a) Top and cross-section view of patterned photoresist layer on a substrate; b) Schematic diagram of the tilted deposition method exploiting the ballistic shadow effect; c) SEM image of rolled-up Ti/Au nanomembranes fabricated according to (b). d) Detailed process flow for rolling up deposited films with high conformity (see text for details); e) optical microscopy image of rolled-up Al_2O_3 nanomembranes obtained following the procedure in (d).

can easily be tuned by the number of rotations, film thickness, and the local environment (not shown here). In contrast to previous reports based on microtube optical resonators from epitaxial layers,[28] our technology offers a low-cost and straightforward alternative to integrate tunable microtube ring resonators from diverse materials and novel material combinations on a single chip for potential applications in, e.g., optical signal processing and optofluidics.

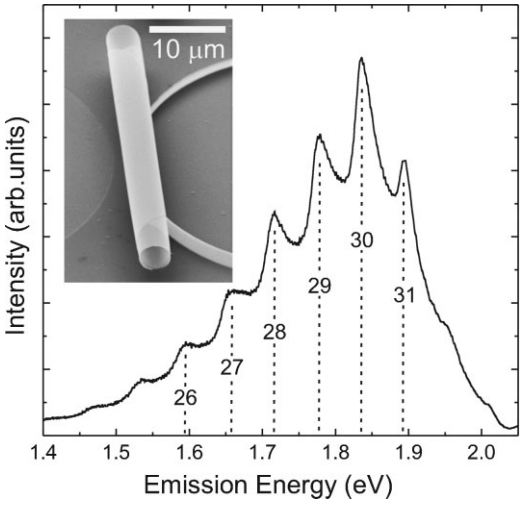

Figure 3. Photoluminescence spectrum of a typical SiO/SiO_2 microtube excited by a 532 nm laser line at room temperature. The inset is an SEM image of a SiO/SiO_2 microtube.

Rolled-up ferromagnetic nanomembranes can be manipulated by external magnetic fields, which render them interesting candidates for fluidic applications in the fields of medicine and biology.[35,36] The rotational response of an actively rotated magnetic object for low Reynolds number environments[37] is given by[36]

$$\langle\dot{\theta}\rangle = \begin{cases} \Omega, & \Omega \le \Omega_c \\ \Omega - \sqrt{\Omega^2 - \Omega_c^2} & \Omega \ge \Omega_c \end{cases} \quad (1)$$

where $\langle\dot{\theta}\rangle$ is the object's average rotation rate and Ω is the driving frequency of the external magnetic field. The critical transition frequency is given by $\Omega_c = mB/\gamma$, where m is the strength of the magnetic moment of the micro-object, B is the external magnetic field amplitude, and γ is the rotational drag coefficient on a liquid surface. For frequencies below Ω_c, the magnetic tube can follow the external field rotation rate but enters a non-linear regime beyond a certain critical frequency, characterized by a retarding action in the rotational dynamics. The inset of Figure 4 shows a sequence of selected high-speed camera frames for a Permalloy ($Ni_{80}Fe_{20}$) tube with 4.5 μm in diameter and 60 μm in length (see center inset) rotating in the non-linear regime under an external magnetic field with a frequency of 6 Hz and on the surface of glycerol at a temperature of 65 °C (see Supporting Information Video I). The grey arrow

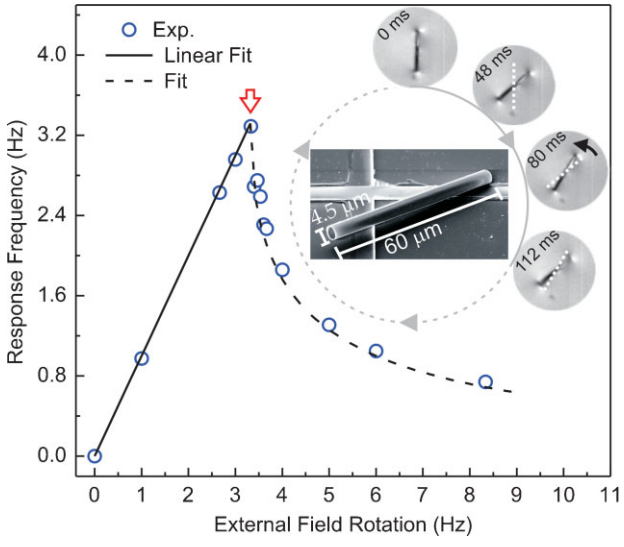

Figure 4. Rotational response of a ferromagnetic microtube on a glycerol solution at 65 °C subject to an external rotating magnetic field of varying frequency. The inset shows selected frames from a high-speed camera video of a ferromagnetic tube with a diameter (length) of 4.5 μm (60 μm). An SEM image of a similar tube is shown in the center.

© 2008 WILEY-VCH Verlag GmbH & Co. KGaA, Weinheim

ADVANCED MATERIALS

indicates the clockwise rotation of the field. For clarity, we drew white dashed lines that represent the tube's previous position to point out the retarding action experienced, in which black arrows indicate the 'rock-in' behavior (anti-rotation). In Figure 4, the symbols represent the experimental data while the solid line is a fit using Equation 1. Based on the critical response frequency (indicated by the empty red arrow in Fig. 4),[35] we determine a rotational drag coefficient (γ) on the liquid surface of around $10^{-6}\,g\cdot cm^2\,s^{-1}$. Knowledge of γ could help to understand small objects moving on a liquid surface, for example, water strider locomotion.[38,39] Since the critical frequency is sensitive to the environment of the tubes, determination of viscosity and detection of organisms, and particles in liquids[35,36] or on liquid surfaces certainly seems feasible.

Self-propelled synthetic micromachines can work autonomously[40] similar to biological micro-organisms converting chemical energy of a local environment into kinetic energy of their motions.[41–45] Due to low Reynolds numbers and Brownian motion,[37,44] a swimming strategy with straight directionality as commonly performed by biological systems[37,46] remains a critical endeavor for engineered machinery on the micro- and nanoscale.[45] In Figure 5a we have fabricated a catalytic tubular microjet using a rolled-up Ti/Fe/Au/Ag multilayer nanomembrane (see inset). Inside the microjet, hydrogen peroxide (H_2O_2) is decomposed into O_2 bubbles and water by a catalytic reaction of H_2O_2 with the inner Ag tube wall. The generation of bubbles, which are thrusted out at one of the openings, causes a highly directional and fast movement of the microjet (see Supporting Information Video II). The Supporting Information Video II also shows that the direction of the microjet can be remotely controlled by an external magnetic field. Figure 5a displays the speed v of the microjet as a function of moving time t. The formation and expansion of each bubble at the tube end generates distinct velocity peaks (marked by black bubbles) of up to $720\,nm\,ms^{-1}$, which are significantly higher than the recorded drift motion at around $150\,nm\,ms^{-1}$ (marked by grey full circles) caused by background fluid flow. After carefully analyzing the video frames taken by a high-speed camera in Figure 5b, we identify a cyclic and asymmetric geometry change from a "single tube" into "a single tube with an attached bubble" and vice versa, which causes the motion of the microjet at low Reynolds number.[37] As shown in Figure 5b, the shape change between Frame 1 (tube without bubble) and 2 (tube with a bubble) causes a one step movement. Further expansion of the bubble (Frame 3), which is still attached to the end of the tube, leads to an additional step of movement. Finally, the bubble increases and detaches from the tube end (Frame 4), which generates a further "discrete" movement. Once detached, the tube retains the original shape (tube without bubble) to be ready for the next motion cycle. Such catalytic microjets could even work without hydrogen peroxide if combined with enzymes glucose oxidase,[45] and thus act as an engineered and well-designed delivery carrier within biological systems.

Cell adhesion and guiding can be controlled by physical and chemical properties of support surfaces, which are normally based on one-dimensional (1D) structures.[47,48] There are only few reports about cell adhesion, guiding, and growth in two-dimensionally (2D) confined micro- or nanostructures.[49] The rolled-up nanomembrane as a well-defined tubular microsystem therefore is a good candidate for cell growth guiding. As shown in the upper part of Figure 6a, yeast cells with an average size of 6 μm are arranged into a well aligned chain in a single Al_2O_3 microtube (upper), which is in direct contrast to the dendritic cell growth occurring on a free surface (lower part of Fig. 6a). More detailed information can be obtained by recording in-situ the guided cell growth. In a relatively large microtube (diameter: ~9.0 μm), the cell pairs (mother cells and their buds marked by yellow arrows) become partially aligned by the microtube *during* growth due to the restricted free space in two dimensions. The influence of the confinement becomes even more striking in a small microtube with a diameter of only 4.5 μm, which is considerably smaller than the natural size of the cells. Still, the cells can enter the tube by elongating their body and replicate themselves strictly along the tube axis. The rolled-up tubes might act as an interesting 3D platform for single cell manipulation, culture, and analysis[50] since the tubes can be easily combined with functionalities of fluidic channels,[27] optical resonators (Fig. 3), remote controls (Fig. 4), catalytic activities (Fig. 5), and/or embedded functional electronic circuits.

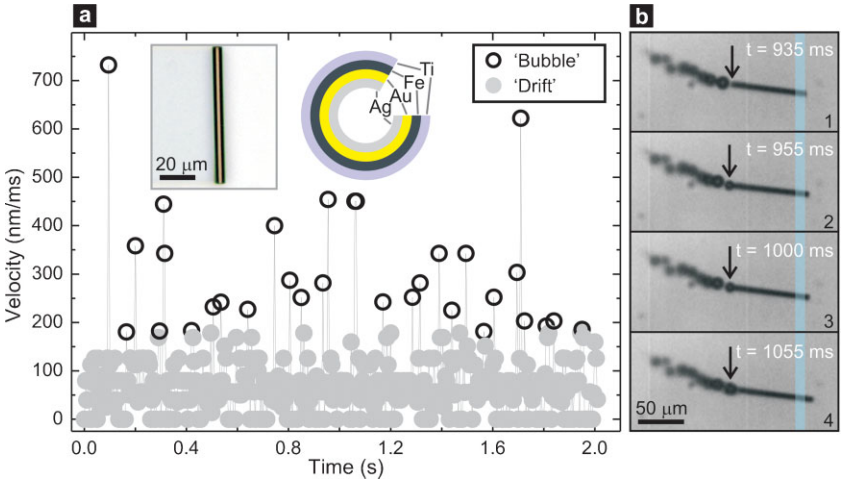

Figure 5. a) Velocity of rolled-up catalytic microjets as a function of time. Left inset shows an optical microscopy image of a single tube and right inset a sketch of the multi-material combination used in this tube. b) Selected video frames of a self-propelled microrocket at different stages of the motion (for more details see text).

In summary, we have developed a generic approach to engineer tubular micro-/

© 2008 WILEY-VCH Verlag GmbH & Co. KGaA, Weinheim

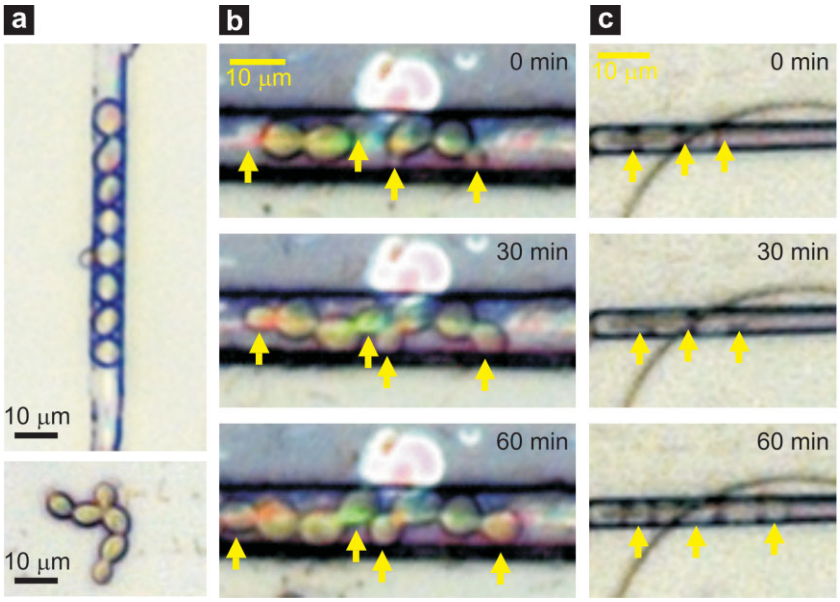

Figure 6. a) Optical images of grown yeast cells in a 2D confined microtube channel (upper part) and on a free surface (lower part). In-situ optical microscopy observation of guided yeast cell growth and budding in a microtube with a diameter of b) ~9.0 μm and c) ~4.5 μm. Yellow arrows mark the growing cells at different times.

nanostructures out of many different materials with tunable diameters and lengths by precisely releasing and rolling up functional nanomembranes on polymers. The technology spans across different scientific fields ranging from photonics to biophysics and has already generated optical ring resonators, magneto-fluidic sensors, remotely controlled microjets and 2D confined channels for cell growth guiding. The unique choice in materials and material combinations together with accurate size, shape and geometry control might open additional objectives towards novel metamaterials,[29] hyperlenses[30] as well as advanced bioanalytic microsystem for the spatial and temporal investigation and control of individual cells.[50]

Experimental

Deposition Methods and Treatments Used for Rolled-up Nanomembranes: Deposition of metals (Pt, Ti, Au, Ag, Pd, Fe, and $Ni_{80}Fe_{20}$) and oxide (SiO and SiO_2) films was carried out by a conventional e-beam evaporator under high vacuum ($<10^{-4}$ Pa). Diamond-like carbon (DLC) films were deposited by plasma immersion ion implantation & deposition (PIII&D) (Plasma Technology Ltd) at room temperature with a substrate bias of −800 V and under a high vacuum ($<10^{-4}$ Pa). We grew Si_xN_y films at a low temperature of 85 °C by PE-CVD using the following parameters: gas flow rate: SiH_4(1.4%)/He(98.6%) = 120 sccm and N_2 = 90 sccm; radio frequency power: 99 W; growth pressure: 11 Pa. Oxide layers such as Al_2O_3, TiO_2, and ZnO were deposited by atomic layer deposition (ALD, Savannah™ 100 from Cambridge NanoTech Inc.) using precursors of trimethylaluminum, titanium(IV) isopropoxide, and Diethylzinc, respectively.

Photoresist layers with a thickness of 1–2 μm were patterned by conventional photolithography methods applying common photoresist materials such as ARP-3510 from Allresist GmbH. Other polymer layers like PMMA (Poly Methyl Methacrylate), PDMS (Polydimethylsiloxane), hydrogel, and others were also tested to confirm the feasibility of our method.

After removing the sacrificial layers in appropriate solvents (acetone, ethanol, and isopropanol from VWR GmbH), critical point drying (CPD 030 Critical Point Dryer from Bal-Tec AG) was applied to dry the rolled-up nanomembranes without structural collapse.

Tube-Based Optical Resonators: We deposited a SiO layer of ~4 nm and then a SiO_2 layer of ~16 nm onto a photoresist layer on Si substrate by using titled e-beam evaporation with a glancing angle of 75°. The dissolving process of the polymer layer by acetone released the films to form a microtube resonator. The optical properties were characterized by micro-photoluminescence spectroscopy at room temperature with an excitation line at 532 nm (Nd-YVO_4 laser).

Magnetic Micro-Oscillators: The single Pd/$Ni_{80}Fe_{20}$/Pd microtube was positioned on top of a 99.9% Merck glycerol solution droplet on a glass slide. The glass slide was placed on top of a conventional hot plate stirrer, which was used to actively rotate the microtube and vary the temperature of the fluid medium. The magnetic field amplitude generated at the sample position was about 12 mT and frequencies from 0.3 Hz up to 8.3 Hz were used to rotate the microtube. The rotational dynamics were recorded at speeds of 30–600 frames per second with a high speed camera (Photonic Science Limited) attached to an optical microscope (Zeiss Axiotech vario).

Catalytic Microjets: Multilayer microtubes of Ti: 10 nm, Fe: 5 nm, Au: 5 nm, and Ag: 10 nm were formed and entirely detached from substrates and placed in an isopropanol solution. A droplet of isopropanol containing microtubes was observed under a microscope followed by an addition of 5% H_2O_2 aqueous solution. Videos were recorded by using the same setup for 'magnetic micro-oscillators'.

Bio-Cell Growth Guided in Microtubes: Rolled-up transparent microtubes of Al_2O_3 or SiO/SiO_2 were used for the cell culture scaffolds. To strengthen the obtained microtubes, a 50-nm-thick Al_2O_3 layer was coated onto both inner and outer surfaces of the microtubes using ALD prior to the cell culture. The budding yeast (bakery yeast) was engaged in the culture experiment and was incubated at 28 °C in YPD medium (Carl Roth GmbH+Co. KG). The cell growth and budding were investigated using a microscope (Zeiss Axiotech vario) connected to a normal camera (Zeiss AxioCam MR).

Received: June 10, 2008

[1] J. H. Ahn, H. S. Kim, K. J. Lee, S. Jeon, S. J. Kang, Y. G. Sun, R. G. Nuzzo, J. A. Rogers, *Science* **2006**, *314*, 1754.
[2] C. Y. Jiang, S. Markutsya, Y. Pikus, V. V. Tsukruk, *Nat. Mater.* **2004**, *3*, 721.
[3] M. M. Robert, L. Klein, D. E. Savage, K. A. Slinker, M. Friesen, G. Celler, M. A. Eriksson, M. G. Lagally, *Nat. Mater.* **2006**, *5*, 388.
[4] C. C. Striemer, T. R. Gaborski, J. L. McGrath, P. M. Fauchet, *Nature* **2007**, *445*, 749.
[5] J. Jin, Y. Wakayama, X. Peng, I. Ichinose, *Nat. Mater.* **2007**, *6*, 686.

 © 2008 WILEY-VCH Verlag GmbH & Co. KGaA, Weinheim

[6] K. E. Mueggenburg, X. M. Lin, R. H. Goldsmith, H. M. Jaeger, *Nat. Mater.* **2007**, *6*, 656.
[7] H. Watanabe, T. Kunitake, *Adv. Mater.* **2007**, *19*, 909.
[8] R. Vendamme, S. Y. Onoue, A. Nakao, T. Kunitake, *Nat. Mater.* **2006**, *5*, 494.
[9] J. C. Meyer, A. K. Geim, M. I. Katsnelson, K. S. Novoselov, T. J. Booth, S. Roth, *Nature* **2007**, *446*, 60.
[10] O. G. Schmidt, N. Schmarje, C. Deneke, C. Muller, N. Y. Jin-Phillipp, *Adv. Mater.* **2001**, *13*, 756.
[11] V. Y. Prinz, V. A. Seleznev, A. K. Gutakovsky, A. V. Chehovskiy, V. V. Preobrazhenskii, M. A. Putyato, T. A. Gavrilova, *Phys. E* **2000**, *6*, 828.
[12] O. G. Schmidt, K. Eberl, *Nature* **2001**, *410*, 168.
[13] Ch. Deneke, U. Zschieschang, H. Klauk, O. G. Schmidt, *Appl. Phys. Lett.* **2006**, *89*, 263110.
[14] V. Luchnikov, O. Sydorenko, M. Stamm, *Adv. Mater.* **2005**, *17*, 1177.
[15] S. Chaieb, M. H. Nayfeh, A. D. Smith, *Appl. Phys. Lett.* **2005**, *87*, 062104.
[16] E. Vekris, G. A. Ozin, V. Kitaev, *Adv. Mater.* **2006**, *18*, 2481.
[17] R. Songmuang, C. Deneke, O. G. Schmidt, *Appl. Phys. Lett.* **2006**, *89*, 223109.
[18] D. Yu, F. Liu, *Nano Lett.* **2007**, *7*, 3046.
[19] M. Huang, C. Boone, M. Roberts, D. E. Savage, M. G. Lagally, N. Shaji, H. Qin, R. Blick, J. A. Nairn, F. Liu, *Adv. Mater.* **2005**, *17*, 2860.
[20] D. J. Bell, L. X. Dong, B. J. Nelson, M. Golling, L. Zhang, D. Grützmacher, *Nano Lett.* **2006**, *6*, 725.
[21] O. G. Schmidt, C. Deneke, Y. M. Manz, C. Müller, *Phys. E* **2002**, *13*, 969.
[22] L. Zhang, L. X. Dong, B. L. Nelson, *Appl. Phys. Lett.* **2008**, *92*, 143110.
[23] Y. F. Mei, D. J. Thurmer, F. Cavallo, S. Kiravittaya, O. G. Schmidt, *Adv. Mater.* **2007**, *19*, 2124.
[24] P. O. Vaccaro, K. Kubota, T. Aida, *Appl. Phys. Lett.* **2001**, *78*, 2852.
[25] H. J. In, S. Kumar, Y. Shao-Horn, G. Barbastathis, *Appl. Phys. Lett.* **2006**, *88*, 083104.
[26] G. J. Meyer, N. L. Dias, R. H. Blick, I. Knezevic, *IEEE Trans. Nanotechnol.* **2007**, *6*, 446.
[27] D. J. Thurmer, C. Deneke, Y. F. Mei, O. G. Schmidt, *Appl. Phys. Lett.* **2006**, *89*, 223507.
[28] R. Songmuang, A. Rastelli, S. Mendach, O. G. Schmidt, *Appl. Phys. Lett.* **2007**, *90*, 091905.
[29] J. B. Pendry, *Science* **2004**, *306*, 1353.
[30] Z. Liu, H. Lee, Y. Xiong, C. Sun, X. Zhang, *Science* **2007**, *315*, 1686.
[31] L. Chen, *Nanomedicine* **2006**, *1*, 365.
[32] C. Deneke, C. Müller, N. Y. Jin-Phillipp, O. G. Schmidt, *Semicond. Sci. Technol.* **2002**, *17*, 1278.
[33] M. F. Doerner, W. D. Nix, *Crit. Rev. Solid State Mater. Sci.* **1988**, *14*, 225.
[34] M. M. Hawkeye, M. J. Brett, *J. Vac. Sci. Technol. A* **2007**, *25*, 1317.
[35] P. A. Valberg, J. P. Butler, *Biophys. J.* **1987**, *52*, 537.
[36] B. H. McNaughton, R. R. Agayan, R. Clarke, R. G. Smith, R. Kopelman, *Appl. Phys. Lett.* **2007**, *91*, 224105.
[37] E. M. Purcell, *Am. J. Phys.* **1977**, *45*, 3.
[38] D. L. Lu, B. Chan, J. W. M. Bush, *Nature* **2003**, *424*, 663.
[39] F. Shi, J. Niu, J. Liu, F. Liu, Z. Wang, X. Q. Feng, X. Zhang, *Adv. Mater.* **2007**, *19*, 2257.
[40] S. Venkataraman, R. M. Dirks, P. W. K. Rothemund, E. Winfree, N. A. Pierce, *Nat. Nanotechnol.* **2007**, *2*, 490.
[41] R. F. Ismagilov, A. Schwartz, N. Bowden, G. M. Whitesides, *Angew. Chem. Int. Ed.* **2002**, *41*, 652.
[42] W. F. Paxton, K. C. Kistler, C. C. Olmeda, A. Sen, S. K. S. Angelo, Y. Cao, T. E. Mallouk, P. E. Lammert, V. H. Crespi, *J. Am. Chem. Soc.* **2004**, *126*, 13424.
[43] S. Fournier-Bidoz, A. C. Arsenault, I. Manners, G. A. Ozin, *Chem. Commun.* **2005**, *441*.
[44] J. R. Howse, R. A. L. Jones, A. J. Ryan, T. Gough, R. Vafabakhsh, R. Golestanian, *Phys. Rev. Lett.* **2007**, *99*, 048102.
[45] D. Pantarotto, W. R. Browne, B. L. Feringa, *Chem. Commun.* **2008**, 1533.
[46] W. R. Browne, B. L. Feringa, *Nat. Nanotechnol.* **2006**, *1*, 25.
[47] R. Kemkemer, S. Jungbauer, D. Kaufmann, H. Gruler, *Biophys. J.* **2006**, *90*, 4701.
[48] S. Y. Park, S. Namgung, B. Kim, J. Im, J. Y. Kim, K. Sun, K. B. Lee, J.-M. Nam, Y. Park, S. Hong, *Adv. Mater.* **2007**, *19*, 2530.
[49] T. Sun, D. Norton, R. J. McKean, J. W. Haycock, A. J. Ryan, S. MacNeil, *Biotechnol. Bioeng.* **2007**, *97*, 1318.
[50] J. EI-Ali, P. K. Sorger, K. F. Jensen, *Nature* **2006**, *442*, 403.

© 2008 WILEY-VCH Verlag GmbH & Co. KGaA, Weinheim